

Adatom engineering magnetic order in superconductors: Applications to altermagnetic superconductivity

Lucas V. Pupim¹ and Mathias S. Scheurer¹

¹*Institute for Theoretical Physics III, University of Stuttgart, 70550 Stuttgart, Germany*

We study theoretically how superlattices based on adatoms on surfaces of unconventional superconductors can be used to engineer novel pairing states that break time-reversal symmetry and exhibit non-trivial magnetic point symmetries. We illustrate this using a square-lattice Hubbard model with d -wave superconductivity and a subleading s -wave state as an example. An adatom superlattice with square-lattice symmetries is shown to stabilize an “orbital-altermagnetic superconductor”, a state that exhibits loop current patterns and associated orbital magnetic moments, which preserve superlattice translations but are odd under four-fold rotations. This state is further characterized by a non-zero Berry curvature quadrupole moment and, upon including spin-orbit coupling, by an altermagnetic spin splitting of the bands and non-trivial spin textures in the superlattice unit cell, with zero net spin moment.

Time-reversal symmetry (\mathcal{T}) plays a special role for superconductivity [1] as it guarantees the degeneracy of Kramers’ partners which can thus form Cooper pairs at weak coupling. This is why pairing in the absence of \mathcal{T} is rare in nature and why the coexistence of magnetism and superconductivity can give rise to a variety of interesting phenomenology, subject of intense current research [2–27]. Similarly, superconductors where the condensate itself spontaneously breaks \mathcal{T} are actively being explored [28–31] and yet there are only a few systems with clear experimental signatures.

To stabilize the microscopic coexistence and probe the intricate interplay of superconductivity and magnetism in a controlled setting, here we propose to employ superlattices built by arranging non-magnetic adatoms on surfaces of materials; these can be assembled with current scanning probe techniques and have been shown to realize a variety of other interesting physics [32–41]. The key ingredient in our work is a correlated substrate featuring unconventional superconductivity, where multiple competing superconducting channels naturally arise. Typically, details of the system, e.g., the chemical potential, determine the leading pairing state. Intuitively, these details can be altered locally by impurities or adatoms so that different superconducting states are favored in different spatial regions of a single sample, and, generically, a complex superposition of the order parameters minimizes the energy [42–44], which in turn breaks \mathcal{T} . Employing this guiding principle, we show that appropriate adatom superlattices lead to complex magnetic order in the superlattice unit cell inside the superconducting phase.

A currently very prominent form of magnetic order is altermagnetism [10–27, 45–92], which is characterized by local moments which average to zero over the lattice—not as a result of translational symmetry (like in an antiferromagnet) but due to (magnetic) point symmetries. For instance, a magnetic texture on the square lattice that is translationally invariant but odd under four-fold rotations C_{4z} (and thus preserves $C_{4z}\mathcal{T}$) defines such an

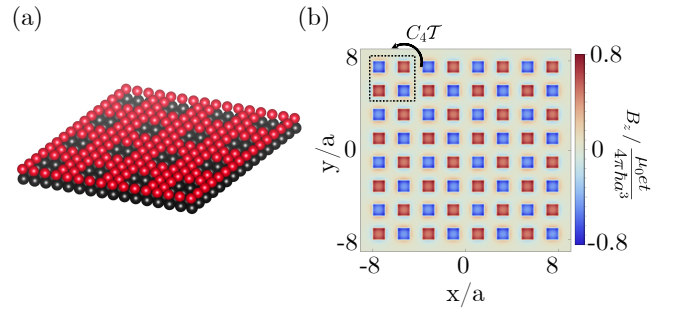


FIG. 1: (a) Schematic of a superconductor surface (black) with a periodic arrangement of non-magnetic adatoms (red) on top. Given that the superconductor has competing orders, time-reversal symmetry can be spontaneously broken and generate loop currents. (b) Out-of-plane magnetic field component due to the loop currents. The dashed square shows the unit cell and we indicate the $C_{4z}\mathcal{T}$ symmetry, characterizing the orbital altermagnet. The chemical potential here is $\mu = -0.5$ and the magnetic field is calculated at $z = 0.1a$.

altermagnetic state [46]. In particular, studying the impact of altermagnetism on superconductivity (assumed to coexist or to be induced via the proximity effect) has taken center stage in the field [10–27].

Our work demonstrates an alternate route to the coexistence of superconductivity and altermagnetism by using adatoms to make the superconducting order parameter to become itself altermagnetic: we show that in the adatom superlattice in Fig. 1(a), which enlarges the unit cell but still exhibits square-lattice symmetries, the superconductor spontaneously breaks \mathcal{T} and C_{4z} but preserves their product; since translations are simultaneously preserved, this defines what we call an “altermagnetic superconductor”. It exhibits local magnetic moments and fields, see Fig. 1(b), coming from orbital currents, which average to zero due to $C_{4z}\mathcal{T}$. Adding spin-orbit coupling (SOC) leads to an altermagnetic spin texture in the unit cell.

Model—Although the above-mentioned scheme of in-

ducing complex magnetic order in an unconventional superconductor via superlattices of non-magnetic adatoms is more generally valid, here we illustrate it employing a square-lattice (lattice constant a) tight-binding model for concreteness. As used in Ref. 42 to describe superconductivity in the cuprates, we take a nearest-neighbor antiferromagnetic ($\mathcal{J} > 0$) spin-spin interaction, $\mathcal{J} \sum_{\langle i,j \rangle} \mathbf{S}_i \cdot \mathbf{S}_j$, where $\mathbf{S}_i = \sum_{\sigma,\sigma'} c_{i,\sigma}^\dagger \boldsymbol{\sigma}_{\sigma,\sigma'} c_{i,\sigma'}$ and $c_{i,\sigma}$ denotes the annihilation operator of an electron on site i and of spin σ . Decoupling the interaction in the spin-singlet channel, we obtain the following mean-field Hamiltonian

$$H = \sum_{i,\sigma} (W_i - \mu) c_{i,\sigma}^\dagger c_{i,\sigma} - \sum_{i,j,\sigma} (t_{i-j} + \delta t_{ij}) c_{i,\sigma}^\dagger c_{j,\sigma} + \left[\sum_{\langle i,j \rangle, \sigma} \Delta_{ij} (c_{i,\uparrow} c_{j,\downarrow} - c_{i,\downarrow} c_{j,\uparrow}) + \text{H.c.} \right]. \quad (1)$$

Here we already allow for adatoms, which break translational symmetry so that in general both the onsite potential and the hopping amplitudes are corrected by spatially modulated contributions, denoted by W_i and δt_{ij} , respectively. As for the bare hoppings, t_{i-j} , we restrict the model to nearest t (and measure all energies in units of t , i.e., $t \equiv 1$) and next-nearest neighbor terms t' with $t' < 0$ [93]. The superconducting order parameter Δ_{ij} is determined by the self-consistency equation $\Delta_{ij} = \mathcal{J} \langle c_{i,\uparrow} c_{j,\downarrow} - c_{i,\downarrow} c_{j,\uparrow} \rangle$; in our numerics, we find Δ_{ij} by iteration until convergence with precision of 10^{-10} .

Without adatoms—We start by discussing the homogeneous limit, $W_i = \delta t_{ij} = 0$. Taking $\mathcal{J} = 1.5$ and $t' = -0.1$, which we will assume throughout the main text, we either find a d -wave or an extended s -wave state as the leading superconductor, depending on the value of the chemical potential, see Fig. 2(a). In both of those states, Δ_{ij} is only non-zero on neighboring sites and invariant under translation, with opposite signs (the same sign) for d -wave (extended s -wave) on bonds related by C_{4z} . Furthermore, for a small but finite range of μ [purple region in Fig. 2(a)], these two orders coexist but with a relative phase of $\pi/2$, realizing an $s \pm id$ superconductor [43]. Intuitively, the non-trivial complex phase between the two orders can be thought as the system's tendency to maximize the excitation gap in this frustrated regime. Recalling the action of time-reversal $\mathcal{T} : \Delta_{ij} \rightarrow \Delta_{ij}^*$, we see that, out of these three superconductors, only the latter $s \pm id$ state breaks \mathcal{T} spontaneously.

Consequences of adatoms—Now, with the role of μ on the nature of superconductivity clarified, we can foresee the consequences of local perturbations caused by adatoms or any other form of impurities [42, 43]. Referring to Appendix A for the discussion of hopping modulations δt_{ij} , here we focus on spatial variations in the onsite potential W_i . It is no surprise that $W_i \neq \text{const.}$ modulates our superconducting pairings Δ_{ij} spatially. How-

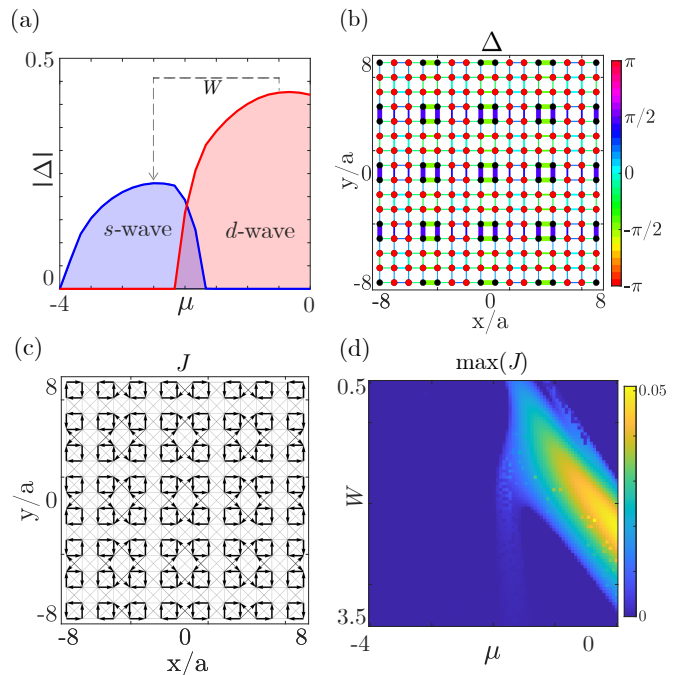


FIG. 2: (a) Phase diagram without adatoms, featuring d -, extended s -wave, and $s \pm id$ superconductivity. The dashed line shows the two phases that are “connected” through a local adatom modulation W . (b) Adatom configuration (red dots) on top of our superconducting lattice (black dots). The colors and width of the bonds represent the complex phase and magnitude of the resulting Δ_{ij} . (c) Respective currents, with only those larger than 5% of the maximum current shown for clarity. (d) Maximal current for different μ and W showing the robustness of the altermagnet phase.

ever, because there are two competing order parameters (s - and d -wave), the spatial modulation can drive the superconducting energetics to break symmetries *spontaneously*. All that is required is to set our system with μ lying in one of the phases and use adatoms capable of shifting the system (locally) to the other.

We exemplify this idea through the dashed line in Fig. 2(a): there, $\mu = -0.5$ so that, without any adatoms, our system is in the d -wave phase—the superconducting order parameter of the cuprate superconductors [94]. A modulation with $W = 2$ tries to drive the sites with adatoms to the s -wave regime. Without coupling between the set of sites with and without adatoms, we would thus obtain regions with extended s - and d -wave superconductivity, respectively. Meanwhile, the coupling between the regions via the hopping terms and \mathcal{J} determines the relative phases and, similar to the homogeneous $s + id$ phase, a configuration with non-trivial complex phases and broken time-reversal symmetry is favored due to the geometric frustration resulting from two order parameters. Moreover, the gradient of Δ (both in magnitude and its complex phase) can create loop currents, which can be viewed as Josephson currents [42]

and will be further studied below. Note that we are not using magnetic adatoms nor fine tuning of the system to the homogeneous $s \pm id$ phase. In fact, the \mathcal{T} -breaking superlattice superconductor also emerges for values of t' where there is no $s \pm id$ phase in the phase diagram of Fig. 2(a).

Adatom superlattice—So far, the intuition we provided aligned with the conclusions in Refs. 42 and 43, where random impurity distributions were studied. Instead, we henceforth explore periodic superlattices created by deliberate placement of adatoms, e.g., the red points in Fig. 2(b) [and also in Fig. 1(a)]. With this arrangement, the unit cell is enlarged by a factor of 4×4 but the associated superlattice has again the full square-lattice symmetry (with atomic translations promoted to superlattice translations). In Fig. 2(b), we further see the resulting order parameter with its different phases and amplitudes varying inside the superlattice unit cell but explicitly invariant under superlattice translation. The non-trivial phases indicate broken \mathcal{T} and the retained symmetries generating the magnetic point-symmetry group are: reflection through the axis (σ_v) and the composite symmetries $\sigma_d \mathcal{T}$ and $C_{4z} \mathcal{T}$ which represent, respectively, reflection through a diagonal and 4-fold rotation followed by time-reversal.

To demonstrate the non-trivial symmetry breaking through gauge-invariant observables, we calculate the currents

$$J_{ij} = -i \frac{e t_{i-j}}{\hbar a^2} \sum_{\sigma} \langle c_{i\sigma}^{\dagger} c_{j\sigma} - \text{H.c.} \rangle \quad (2)$$

on all bonds (ij). The currents are found to be of the order of $\sim 0.04 \frac{et}{\hbar a^2}$ and their spatial pattern is shown in Fig. 2(c). In agreement with the above symmetry analysis of the superconductor, they preserve superlattice translations and σ_v but are odd under C_{4v} and σ_d .

Note that all orbital currents vanish, $J_{ij} = 0$, in the homogeneous $s \pm id$ state as follows straightforwardly from the combination of magnetic point symmetries and invariance under translation by a single square-lattice site [95–97]. We also emphasize that the emergence of these orbital currents is a robust effect that does not require fine tuning. In Fig. 2(d), we plot the maximum current on the lattice as a function of μ and W for the same adatom superlattice as in Fig. 2(b) and find an extended regime with $J_{ij} \neq 0$ and the same magnetic point symmetries as above.

Altermagnetic Superconductor—Given the shape and arrangement of the orbital current loops, it is natural to associate them with Ising-like magnetic moments. To corroborate our intuition and compute the local magnetic field profile that can be measured in scanning magnetometry experiments, we consider each nearest- and next-nearest-neighbor link as a one-dimensional wire and apply the Biot-Savart law. As we can see in Fig. 1(b), the

resulting magnetic field exhibits well-separated regions of alternating sign arranged in a checkerboard-like pattern. This pattern again reveals the non-trivial magnetic point symmetries. Keeping the superlattice unit cell in mind, which is indicated as dashed black square in Fig. 1(b), the regions of opposite sign of the magnetic field are not related by translational symmetry (like in an antiferromagnet) but by C_{4z} . As such, we refer to this superconductor as an *orbital altermagnet*, where “orbital” refers to the fact that symmetries are broken in the orbital channel and the ground state is spin rotation invariant. The “altermagnetic spin liquid”, recently discussed in Ref. 92, is conceptually related since it also exhibits altermagnetic orbital currents while being spin-rotation invariant; however, the physical realizations—quantum disordering a non-coplanar magnet vs. spatial frustration in a superconducting superlattice—differ significantly.

We note that these results are not restricted to the specific superlattice in Fig. 2(b). It is also possible to observe this altermagnetic phase with different (bigger) superlattice unit cell sizes, which could help to probe the magnetic moments through magnetometry techniques, since it would require less spatial resolution. Deforming the square superlattice into a rectangular one is also possible, although now the magnetic point-symmetry group is reduced to C_{2v} ; the residual σ_v reflection symmetry is still sufficient to guarantee the vanishing of the total magnetic moment per unit cell. In addition, modulating the hopping, $\delta t_{ij} \neq 0$ in Eq. (1), instead of the chemical potential, or starting with a different leading pairing state lead to similar results (see Appendix).

To delve deeper into the superlattice superconductor, let us look into its band structure. To this end, we come back to the superlattice and order parameter of Fig. 1(a) and Fig. 2(b), where each superlattice unit cell contains $N = 4 \times 4$ sites of the original square lattice. Each site i within a given unit cell \mathbf{R} is associated with a Nambu spinor $\psi_i(\mathbf{R}) = [c_{i+\mathbf{R},\uparrow} \ c_{i+\mathbf{R},\downarrow} \ c_{i+\mathbf{R},\uparrow}^{\dagger} \ c_{i+\mathbf{R},\downarrow}^{\dagger}]$, allowing us to subsequently describe superconductivity in the whole unit cell by $\Psi_{\mathbf{R}} = [\psi_1(\mathbf{R}) \ \psi_2(\mathbf{R}) \ \dots \ \psi_i(\mathbf{R}) \ \dots \ \psi_N(\mathbf{R})]$. We can now use this formulation to write

$$H = \sum_{\mathbf{R}} (\Psi_{\mathbf{R}}^{\dagger} h_0 \Psi_{\mathbf{R}} + \sum_{\nu=x,y} [\Psi_{\mathbf{R}}^{\dagger} T_{\nu} \Psi_{\mathbf{R}+\hat{e}_{\nu}} + \text{H.c.}]), \quad (3)$$

where all the terms from Eq. (1) that represent processes within the unit cell are contained in h_0 and T_{ν} represents the hopping and pairing from one superlattice unit cell \mathbf{R} to an adjacent cell at $\mathbf{R} + \hat{e}_{\nu}$ with $\nu = x, y$. After Fourier transformation with respect to \mathbf{R} , $\Psi_{\mathbf{R}} = \sum_{\mathbf{k}} e^{-i\mathbf{k}\mathbf{R}} \tilde{\Psi}_{\mathbf{k}}$, and diagonalization of the $N \times N$ Bogoliubov-de Gennes Hamiltonian, we obtain the superconducting bands in Fig. 3(a). Since the spectrum is particle-hole symmetric, we just plot positive energy bands for clarity. Only at Γ and M (which retain the full magnetic point group of the superconductor) are enough symmetries present to

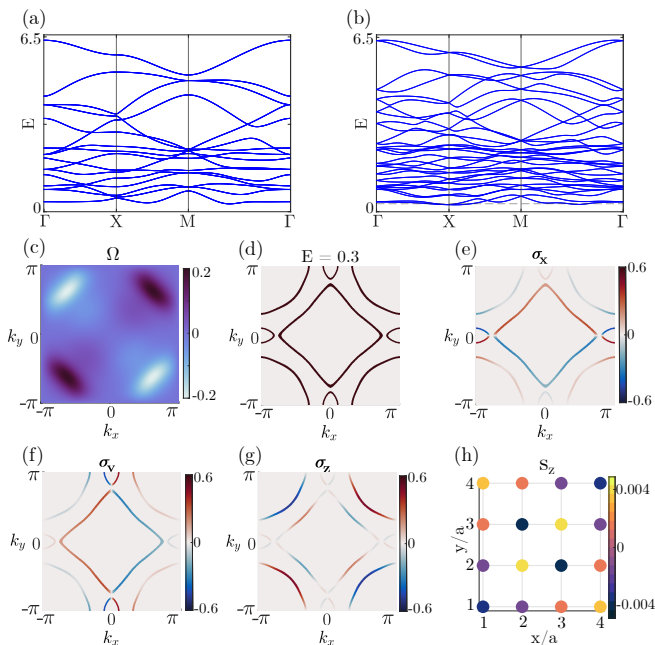


FIG. 3: Band structure of the altermagnetic superconductor (a) without and (b) with SOC ($\lambda = 0.2$). (c) Composite Berry curvature of the occupied bands for $\lambda = 0$. (d) Energy cut at $E = 0.6$ from (b) and the respective spin texture (e-g) for the indicated spin components, which inherit the symmetries of the orbital altermagnet via $\lambda \neq 0$. (h) Local spins in the unit cell. They also obey the orbital altermagnet symmetries. The net spin in the unit cell vanishes, as expected for an altermagnet. We use $\mu = -0.25$.

guarantee two-dimensional representations leading to degeneracies of bands; these are lifted away from these two high-symmetry points.

Since there is no \mathbf{k} -space-local anti-unitary symmetry (like $C_{2z}\mathcal{T}$, which is broken spontaneously by the superconductor), the Berry curvature $\Omega(\mathbf{k})$ can be non-zero. However, $C_4\mathcal{T}$ enforces $\Omega(\mathbf{k}) = -\Omega(C_{4z}\mathbf{k})$ such that both the Chern number (monopole) and the Berry curvature dipole moment have to vanish. The first non-zero moment is thus the Berry curvature quadrupole, which is confirmed by our explicit calculation [98, 99] of the composite Berry curvature Ω for the ground state, shown in Fig. 3(c). Our result further obeys the additional constraints $\Omega(\mathbf{k}) = \Omega(\sigma_j\mathbf{k}) = -\Omega(\sigma_v\mathbf{k})$ coming from the remaining magnetic point symmetries. While C_4 and σ_v would have to be broken (e.g., by nematic order) to obtain a finite Chern number and, thus, finite thermal Hall effect, higher moments of the Berry curvature also bring observable signatures in non-linear transport, even with a trivial Chern number [63, 100–103]. For our case of a superconductor, the non-zero Berry quadrupole moment can be probed via the non-linear thermal Hall effect and non-linear Nernst effect [100], which are observed under a temperature gradient.

Spin-orbit coupling—We can make the spin channel inherit the altermagnetic structure, which was previously an entirely orbital effect, by adding SOC to our model. For concreteness, here we discuss a Rashba-like term [104] which reads as $i\lambda \left(c_{(x,y)}^\dagger \sigma_x c_{(x,y+1)} - c_{(x,y)}^\dagger \sigma_y c_{(x+1,y)} \right) + \text{H.c.}$ and respects all symmetries of the underlying square lattice and \mathcal{T} . Including the respective contributions in Eq. (3), we obtain the corresponding Bogoliubov bands shown in Fig. 3(b). We can see that SOC splits the previously spin-degenerate bands everywhere but at the high-symmetry points.

We can further see this splitting through an energy cut in Fig. 3(d), and in (e) and (f) where we show the in-plane spin polarizations at the given energy. Note that the presence of C_{2z} symmetry implies that the in-plane spin polarizations are always even under \mathcal{T} . They, thus, represent the Rashba SOC and do not contain any altermagnetic contribution. This is different for the out-of-plane spin component, which has to be odd under \mathcal{T} and, hence, captures the altermagnetic part of the spin splitting, inherited from the superconductor. Indeed, we can see in Fig. 3(g) that this component exhibits the sign changes under C_{4z} with nodes pinned by σ_v along the momentum axes, characteristic of a square-lattice altermagnet. Hence, by adding an in-plane SOC to our (out-of-plane) orbital altermagnet, we obtain an out-of-plane spin altermagnet. This result is true for all bands, but the degree of out-of-plane polarization can vary (roughly) from 10^{-4} to 0.6 depending on the energy cut.

Interestingly, a non-zero local spin expectation value, $\langle S_i^z \rangle \neq 0$, at a given site i , is also inherited from the orbital altermagnetic superconductor when including SOC, $\lambda \neq 0$. In Fig. 3(h), we show the intra-unit cell behavior of the out-of-plane component $\langle S_i^z \rangle$, which exhibits a non-trivial spatial texture that, by virtue of being odd under C_{4z} , has vanishing total magnetization.

Conclusion and outlook—In this work, we demonstrated how superlattices of non-magnetic adatoms can be used to design non-trivial symmetry breaking in superconductors with multiple competing order parameters. In our concrete square-lattice computation, we showed that this can stabilize a novel altermagnetic superconductor with interesting and experimentally accessible properties. More generally, this approach can be applied to a variety of different superconducting systems which, apart from designing other symmetry-reduced superconductors of interest, can also be used to look “below the surface” of the leading superconducting state and uncover competing phases. At the same time, it can provide a tool for investigating the origin of signatures of broken time-reversal symmetry in certain superconducting compounds [28].

ACKNOWLEDGMENTS

The authors acknowledge funding by the European Union (ERC-2021-STG, Project 101040651—SuperCorr). Views and opinions expressed are however those of the authors only and do not necessarily reflect those of the European Union or the European Research

Council Executive Agency. Neither the European Union nor the granting authority can be held responsible for them. M.S.S. further acknowledges support by grant NSF PHY-2309135 for his stay at the Kavli Institute for Theoretical Physics (KITP) where part of the research was carried out. The authors thank J. Sobral and S. Banerjee for fruitful discussions.

-
- [1] P. Anderson, “Theory of dirty superconductors,” *Journal of Physics and Chemistry of Solids* **11**, 26 (1959).
- [2] F. Ando, Y. Miyasaka, T. Li, J. Ishizuka, T. Arakawa, Y. Shiota, T. Moriyama, Y. Yanase, and T. Ono, “Observation of superconducting diode effect,” *Nature* **584**, 373 (2020).
- [3] A. Daido, Y. Ikeda, and Y. Yanase, “Intrinsic Superconducting Diode Effect,” *Physical Review Letters* **128**, 037001 (2022).
- [4] J. J. He, Y. Tanaka, and N. Nagaosa, “A phenomenological theory of superconductor diodes,” *New Journal of Physics* **24**, 053014 (2022).
- [5] N. F. Q. Yuan and L. Fu, “Supercurrent diode effect and finite-momentum superconductors,” *Proceedings of the National Academy of Sciences* **119**, e2119548119 (2022).
- [6] H. D. Scammell, J. I. A. Li, and M. S. Scheurer, “Theory of zero-field superconducting diode effect in twisted trilayer graphene,” *2D Materials* **9**, 025027 (2022).
- [7] M. Christos, S. Sachdev, and M. S. Scheurer, “Nodal band-off-diagonal superconductivity in twisted graphene superlattices,” *Nature Communications* **14**, 7134 (2023).
- [8] P. H. Wilhelm, A. M. Läuchli, and M. S. Scheurer, “A Novel Perspective on Ideal Chern Bands with Strong Short-Range Repulsion: Applications to Correlated Metals, Superconductivity, and Topological Order,” arXiv e-prints (2024), [arXiv:2406.09505](https://arxiv.org/abs/2406.09505) [cond-mat.str-el].
- [9] T. Han, Z. Lu, Y. Yao, L. Shi, J. Yang, J. Seo, S. Ye, Z. Wu, M. Zhou, H. Liu, G. Shi, Z. Hua, K. Watanabe, T. Taniguchi, P. Xiong, L. Fu, and L. Ju, “Signatures of chiral superconductivity in rhombohedral graphene,” (2024), [arXiv:2408.15233](https://arxiv.org/abs/2408.15233).
- [10] G. Sim and J. Knolle, “Pair Density Waves and Supercurrent Diode Effect in Altermagnets,” arXiv e-prints (2024), [arXiv:2407.01513](https://arxiv.org/abs/2407.01513) [cond-mat.supr-con].
- [11] V. S. de Carvalho and H. Freire, “Unconventional superconductivity in altermagnets with spin-orbit coupling,” arXiv e-prints (2024), [arXiv:2409.10712](https://arxiv.org/abs/2409.10712) [cond-mat.supr-con].
- [12] I. I. Mazin, “Notes on altermagnetism and superconductivity,” 2203.05000.
- [13] A. Bose, S. Vadnais, and A. Paramakanti, “Altermagnetism and superconductivity in a multiorbital t-J model,” arXiv e-prints (2024), [arXiv:2403.17050](https://arxiv.org/abs/2403.17050) [cond-mat.str-el].
- [14] C. Xu, S. Wu, G.-X. Zhi, G. Cao, J. Dai, C. Cao, X. Wang, and H.-Q. Lin, “Frustrated Altermagnetism and Charge Density Wave in Kagome Superconductor CsCr3Sb5,” arXiv e-prints (2023), [arXiv:2309.14812](https://arxiv.org/abs/2309.14812) [cond-mat.supr-con].
- [15] S. Banerjee and M. S. Scheurer, “Altermagnetic superconducting diode effect,” *Phys. Rev. B* **110**, 024503 (2024).
- [16] H. O. Jeschke, M. Shimizu, and I. I. Mazin, “Highly unusual, doubly-strongly-correlated, altermagnetic, 3D analogue of parent compounds of high-Tc cuprates,” 2403.02201.
- [17] C. W. J. Beenakker and T. Vakhstel, “Phase-shifted Andreev levels in an altermagnet Josephson junction,” *Physical Review B* **108**, 075425 (2023).
- [18] B. Brekke, A. Brataas, and A. Sudbø, “Two-dimensional altermagnets: Superconductivity in a minimal microscopic model,” *Physical Review B* **108**, 224421 (2023).
- [19] D. Chakraborty and A. M. Black-Schaffer, “Zero-field finite-momentum and field-induced superconductivity in altermagnets,” (2023), [arxiv:2309.14427](https://arxiv.org/abs/2309.14427) [cond-mat].
- [20] J. A. Ouassou, A. Brataas, and J. Linder, “Dc Josephson Effect in Altermagnets,” *Physical Review Letters* **131**, 076003 (2023).
- [21] D. Zhu, Z.-Y. Zhuang, Z. Wu, and Z. Yan, “Topological superconductivity in two-dimensional altermagnetic metals,” *Phys. Rev. B* **108**, 184505 (2023).
- [22] Y.-X. Li and C.-C. Liu, “Majorana corner modes and tunable patterns in an altermagnet heterostructure,” *Phys. Rev. B* **108**, 205410 (2023).
- [23] S. A. A. Ghorashi, T. L. Hughes, and J. Cano, “Altermagnetic Routes to Majorana Modes in Zero Net Magnetization,” *Phys. Rev. Lett.* **133**, 106601 (2024).
- [24] C. Sun, A. Brataas, and J. Linder, “Andreev reflection in altermagnets,” *Phys. Rev. B* **108**, 054511 (2023).
- [25] H. G. Giil and J. Linder, “Superconductor-altermagnet memory functionality without stray fields,” *Phys. Rev. B* **109**, 134511 (2024).
- [26] Q. Cheng and Q.-F. Sun, “Orientation-dependent josephson effect in spin-singlet superconductor/altermagnet/spin-triplet superconductor junctions,” *Phys. Rev. B* **109**, 024517 (2024).
- [27] M. Wei, L. Xiang, F. Xu, L. Zhang, G. Tang, and J. Wang, “Gapless superconducting state and mirage gap in altermagnets,” *Phys. Rev. B* **109**, L201404 (2024).
- [28] S. K. Ghosh, M. Smidman, T. Shang, J. F. Annett, A. D. Hillier, J. Quintanilla, and H. Yuan, “Recent progress on superconductors with time-reversal symmetry breaking,” *Journal of Physics: Condensed Matter* **33**, 033001 (2020).

- [29] X. Wu, F. Ming, T. S. Smith, G. Liu, F. Ye, K. Wang, S. Johnston, and H. H. Weitering, “Superconductivity in a hole-doped mott-insulating triangular adatom layer on a silicon surface,” *Phys. Rev. Lett.* **125**, 117001 (2020).
- [30] F. Ming, X. Wu, C. Chen, K. D. Wang, P. Mai, T. A. Maier, J. Strockoz, J. Venderbos, C. González, J. Ortega, *et al.*, “Evidence for chiral superconductivity on a silicon surface,” *Nature Physics* **19**, 500 (2023).
- [31] S. Y. F. Zhao, X. Cui, P. A. Volkov, H. Yoo, S. Lee, J. A. Gardener, A. J. Akey, R. Engelke, Y. Ronen, R. Zhong, G. Gu, S. Plugge, T. Tummuru, M. Kim, M. Franz, J. H. Pixley, N. Poccia, and P. Kim, “Time-reversal symmetry breaking superconductivity between twisted cuprate superconductors,” *Science* **382**, 1422 (2023).
- [32] M. N. Huda, S. Kezilebieke, and P. Liljeroth, “Designer flat bands in quasi-one-dimensional atomic lattices,” *Phys. Rev. Res.* **2**, 043426 (2020).
- [33] S. N. Kempkes, M. R. Slot, S. E. Freney, S. J. Zevenhuizen, D. Vanmaekelbergh, I. Swart, and C. M. Smith, “Design and characterization of electrons in a fractal geometry,” *Nature physics* **15**, 127 (2019).
- [34] S. Kempkes, M. Slot, J. van Den Broeke, P. Capiod, W. Benalcazar, D. Vanmaekelbergh, D. Bercioux, I. Swart, and C. Morais Smith, “Robust zero-energy modes in an electronic higher-order topological insulator,” *Nature Materials* **18**, 1292 (2019).
- [35] M. R. Slot, T. S. Gardenier, P. H. Jacobse, G. C. Van Miert, S. N. Kempkes, S. J. Zevenhuizen, C. M. Smith, D. Vanmaekelbergh, and I. Swart, “Experimental realization and characterization of an electronic lieb lattice,” *Nature physics* **13**, 672 (2017).
- [36] T. S. Gardenier, J. J. van den Broeke, J. R. Moes, I. Swart, C. Delerue, M. R. Slot, C. M. Smith, and D. Vanmaekelbergh, “p orbital flat band and dirac cone in the electronic honeycomb lattice,” *ACS Nano* **14**, 13638 (2020), PMID: 32991147.
- [37] M. R. Slot, S. N. Kempkes, E. J. Knol, W. M. J. van Weerdenburg, J. J. van den Broeke, D. Wegner, D. Vanmaekelbergh, A. A. Khajetoorians, C. Morais Smith, and I. Swart, “p-band engineering in artificial electronic lattices,” *Phys. Rev. X* **9**, 011009 (2019).
- [38] R. Drost, T. Ojanen, A. Harju, and P. Liljeroth, “Topological states in engineered atomic lattices,” *Nature Physics* **13**, 668 (2017).
- [39] M. Yahyavi, B. Hetényi, and B. Tanatar, “Generalized aubry-andré-harper model with modulated hopping and p-wave pairing,” *Phys. Rev. B* **100**, 064202 (2019).
- [40] Q.-B. Zeng, S. Chen, and R. Lü, “Generalized aubry-andré-harper model with p-wave superconducting pairing,” *Phys. Rev. B* **94**, 125408 (2016).
- [41] J. Yu, E. Lauricella, M. Elsayed, K. Shepherd, N. S. Nichols, T. Lombardi, S. W. Kim, C. Wexler, J. M. Vanegas, T. Lakoba, V. N. Kotov, and A. Del Maestro, “Two-dimensional bose-hubbard model for helium on graphene,” *Phys. Rev. B* **103**, 235414 (2021).
- [42] Z.-X. Li, S. A. Kivelson, and D.-H. Lee, “Superconductor-to-metal transition in overdoped cuprates,” *npj Quantum Materials* **6**, 36 (2021).
- [43] C. N. Breið, P. J. Hirschfeld, and B. M. Andersen, “Supercurrents and spontaneous time-reversal symmetry breaking by nonmagnetic disorder in unconventional superconductors,” *Phys. Rev. B* **105**, 014504 (2022).
- [44] M. S. Scheurer, D. F. Agterberg, and J. Schmalian, “Selection rules for cooper pairing in two-dimensional interfaces and sheets,” *npj Quantum Materials* **2**, 9 (2017).
- [45] L.-D. Yuan, Z. Wang, J.-W. Luo, E. I. Rashba, and A. Zunger, “Giant momentum-dependent spin splitting in centrosymmetric low- Z antiferromagnets,” *Physical Review B* **102**, 014422 (2020).
- [46] L. Šmejkal, J. Sinova, and T. Jungwirth, “Beyond Conventional Ferromagnetism and Antiferromagnetism: A Phase with Nonrelativistic Spin and Crystal Rotation Symmetry,” *Physical Review X* **12**, 031042 (2022).
- [47] L. Šmejkal, J. Sinova, and T. Jungwirth, “Emerging Research Landscape of Altermagnetism,” *Physical Review X* **12**, 040501 (2022).
- [48] K.-H. Ahn, A. Hariki, K.-W. Lee, and J. Kuneš, “Antiferromagnetism in RuO₂ as d-wave Pomeranchuk instability,” *Physical Review B* **99**, 184432 (2019).
- [49] S. Bhowal and N. A. Spaldin, “Ferroically Ordered Magnetic Octupoles in d-Wave Altermagnets,” *Phys. Rev. X* **14**, 011019 (2024).
- [50] G. Cuono, R. M. Sattigeri, J. Skolimowski, and C. Autieri, “Orbital-selective altermagnetism and correlation-enhanced spin-splitting in transition metal oxides,” *Journal of Magnetism and Magnetic Materials* **586**, 171163 (2023), arxiv:2306.17497 [cond-mat].
- [51] Y. Guo, H. Liu, O. Janson, I. C. Fulga, J. van den Brink, and J. I. Facio, “Spin-split collinear antiferromagnets: A large-scale ab-initio study,” *Materials Today Physics* **32**, 100991 (2023).
- [52] T. A. Maier and S. Okamoto, “Weak-coupling theory of neutron scattering as a probe of altermagnetism,” *Physical Review B* **108**, L100402 (2023).
- [53] I. I. Mazin, “Altermagnetism in MnTe: Origin, predicted manifestations, and routes to detwinning,” *Physical Review B* **107**, L100418 (2023).
- [54] V. Oganesyan, S. A. Kivelson, and E. Fradkin, “Quantum theory of a nematic Fermi fluid,” *Physical Review B* **64**, 195109 (2001).
- [55] T. Sato, S. Haddad, I. C. Fulga, F. F. Assaad, and J. van den Brink, “Altermagnetic Anomalous Hall Effect Emerging from Electronic Correlations,” *Phys. Rev. Lett.* **133**, 086503 (2024).
- [56] C. R. W. Steward, R. M. Fernandes, and J. Schmalian, “Dynamic paramagnon-polarons in altermagnets,” *Physical Review B* **108**, 144418 (2023).
- [57] I. Turek, “Altermagnetism and magnetic groups with pseudoscalar electron spin,” *Physical Review B* **106**, 094432 (2022).
- [58] I. I. Mazin, K. Koepernik, M. D. Johannes, R. González-Hernández, and L. Šmejkal, “Prediction of unconventional magnetism in doped FeSb₂,” *Proceedings of the National Academy of Sciences* **118**, e2108924118 (2021).
- [59] S. Hayami, Y. Yanagi, and H. Kusunose, “Momentum-dependent spin splitting by collinear antiferromagnetic ordering,” *Journal of the Physical Society of Japan* **88**, 123702 (2019).
- [60] L. Šmejkal, R. González-Hernández, T. Jungwirth, and J. Sinova, “Crystal time-reversal symmetry breaking and spontaneous hall effect in collinear antiferromag-

- nets,” *Science Advances* **6**, eaaz8809 (2020).
- [61] P. Das, V. Leeb, J. Knolle, and M. Knap, “Realizing Altermagnetism in Fermi-Hubbard Models with Ultracold Atoms,” *Phys. Rev. Lett.* **132**, 263402 (2024).
- [62] A. Fakhredine, R. M. Sattigeri, G. Cuono, and C. Autieri, “Interplay between altermagnetism and nonsymmorphic symmetries generating large anomalous Hall conductivity by semi-Dirac points induced anticrossings,” *Physical Review B* **108**, 115138 (2023).
- [63] Y. Fang, J. Cano, and S. A. A. Ghorashi, “Quantum geometry induced nonlinear transport in altermagnets,” *Phys. Rev. Lett.* **133**, 106701 (2024).
- [64] V. Leeb, A. Mook, L. Šmejkal, and J. Knolle, “Spontaneous Formation of Altermagnetism from Orbital Ordering,” *Phys. Rev. Lett.* **132**, 236701 (2024).
- [65] I. Mazin, R. González-Hernández, and L. Šmejkal, “Induced Monolayer Altermagnetism in $\text{MnP}(\text{S,Se})_3$ and FeSe ,” (2023), [arxiv:2309.02355](https://arxiv.org/abs/2309.02355) [cond-mat].
- [66] L. Šmejkal, A. Marmodoro, K.-H. Ahn, R. González-Hernández, I. Turek, S. Mankovsky, H. Ebert, S. W. D’Souza, O. Šipr, J. Sinova, and T. Jungwirth, “Chiral Magnons in Altermagnetic RuO_2 ,” *Physical Review Letters* **131**, 256703 (2023).
- [67] C. Sun and J. Linder, “Spin pumping from a ferromagnetic insulator into an altermagnet,” *Physical Review B* **108**, L140408 (2023).
- [68] Z.-F. Gao, S. Qu, B. Zeng, Y. Liu, J.-R. Wen, H. Sun, P.-J. Guo, and Z.-Y. Lu, “AI-accelerated Discovery of Altermagnetic Materials,” (2023), [arxiv:2311.04418](https://arxiv.org/abs/2311.04418) [cond-mat, physics:physics].
- [69] X. Zhou, W. Feng, R.-W. Zhang, L. Šmejkal, J. Sinova, Y. Mokrousov, and Y. Yao, “Crystal thermal transport in altermagnetic RuO_2 ,” *Phys. Rev. Lett.* **132**, 056701 (2024).
- [70] R. M. Fernandes, V. S. de Carvalho, T. Birol, and R. G. Pereira, “Topological transition from nodal to nodeless zeeman splitting in altermagnets,” *Phys. Rev. B* **109**, 024404 (2024).
- [71] S.-B. Zhang, L.-H. Hu, and T. Neupert, “Finite-momentum Cooper pairing in proximitized altermagnets,” *Nat. Commun.* **15**, 1 (2024).
- [72] D. S. Antonenko, R. M. Fernandes, and J. W. F. Venderbos, “Mirror chern bands and weyl nodal loops in altermagnets,” (2024), [arXiv:2402.10201](https://arxiv.org/abs/2402.10201) [cond-mat.mes-hall].
- [73] Y. Yu, H.-G. Suh, M. Roig, and D. F. Agterberg, “Altermagnetism from coincident van hove singularities: application to $\kappa\text{-cl}$,” (2024), [arXiv:2402.05180](https://arxiv.org/abs/2402.05180) [cond-mat.str-el].
- [74] P. A. McClarty and J. G. Rau, “Landau theory of altermagnetism,” *Phys. Rev. Lett.* **132**, 176702 (2024).
- [75] K. V. Yershov, V. P. Kravchuk, M. Daghofer, and J. van den Brink, “Fluctuation-induced piezomagnetism in local moment altermagnets,” *Phys. Rev. B* **110**, 144421 (2024).
- [76] Q. Cui, B. Zeng, P. Cui, T. Yu, and H. Yang, “Efficient spin seebeck and spin nernst effects of magnons in altermagnets,” *Phys. Rev. B* **108**, L180401 (2023).
- [77] P. M. Cõnsoli and M. Vojta, “ $\text{SU}(3)$ altermagnetism: Lattice models, chiral magnons, and flavor-split bands,” arXiv e-prints (2024), [arXiv:2402.18629](https://arxiv.org/abs/2402.18629) [cond-mat.str-el].
- [78] T. Jungwirth, R. M. Fernandes, J. Sinova, and L. Šmejkal, “Altermagnets and beyond: Nodal magnetically-ordered phases,” arXiv e-prints (2024), [arXiv:2409.10034](https://arxiv.org/abs/2409.10034) [cond-mat.mtrl-sci].
- [79] J. Öiké, K. Shinada, and R. Peters, “Nonlinear Magnetoelectric Effect under Magnetic Octupole Order: Its Application to a d -Wave Altermagnet and a Pyrochlore Lattice with All-In/All-Out Magnetic Order,” arXiv e-prints (2024), [arXiv:2407.15836](https://arxiv.org/abs/2407.15836) [cond-mat.mtrl-sci].
- [80] M. Roig, A. Kreisel, Y. Yu, B. M. Andersen, and D. F. Agterberg, “Minimal models for altermagnetism,” *Phys. Rev. B* **110**, 144412 (2024).
- [81] M. Zhao, W.-W. Yang, X. Guo, H.-G. Luo, and Y. Zhong, “Altermagnetism in Heavy Fermion Systems,” arXiv e-prints (2024), [arXiv:2407.05220](https://arxiv.org/abs/2407.05220) [cond-mat.str-el].
- [82] T. Aoyama and K. Ohgushi, “Piezomagnetic properties in altermagnetic MnTe ,” *Phys. Rev. Mater.* **8**, L041402 (2024).
- [83] H. Bai, Y. C. Zhang, Y. J. Zhou, P. Chen, C. H. Wan, L. Han, W. X. Zhu, S. X. Liang, Y. C. Su, X. F. Han, F. Pan, and C. Song, “Efficient Spin-to-Charge Conversion via Altermagnetic Spin Splitting Effect in Antiferromagnet RuO_2 ,” *Physical Review Letters* **130**, 216701 (2023).
- [84] J. Krempaský, L. Šmejkal, S. W. D’Souza, M. Hajlaoui, G. Springholz, K. Uhlířová, F. Alarab, P. C. Constantinou, V. Strocov, D. Usanov, W. R. Pudelko, R. González-Hernández, A. Birk Hellenes, Z. Jansa, H. Reichlová, Z. Šobáň, R. D. Gonzalez Betancourt, P. Wadley, J. Sinova, D. Krieger, J. Minár, J. H. Dil, and T. Jungwirth, “Altermagnetic lifting of Kramers spin degeneracy,” *Nature* **626**, 517 (2024).
- [85] S. Lee, S. Lee, S. Jung, J. Jung, D. Kim, Y. Lee, B. Seok, J. Kim, B. G. Park, L. Šmejkal, C.-J. Kang, and C. Kim, “Broken Kramers Degeneracy in Altermagnetic MnTe ,” *Phys. Rev. Lett.* **132**, 036702 (2024).
- [86] S. Reimers, L. Odenbreit, L. Šmejkal, V. N. Strocov, P. Constantinou, A. B. Hellenes, R. Jaeschke Ubiergo, W. H. Campos, V. K. Bharadwaj, A. Chakraborty, T. Denneulin, W. Shi, R. E. Dunin-Borkowski, S. Das, M. Kläui, J. Sinova, and M. Jourdan, “Direct observation of altermagnetic band splitting in CrSb thin films,” *Nat. Commun.* **15**, 1 (2024).
- [87] Z. Feng, X. Zhou, L. Šmejkal, L. Wu, Z. Zhu, H. Guo, R. González-Hernández, X. Wang, H. Yan, P. Qin, X. Zhang, H. Wu, H. Chen, Z. Meng, L. Liu, Z. Xia, J. Sinova, T. Jungwirth, and Z. Liu, “An anomalous Hall effect in altermagnetic ruthenium dioxide,” *Nature Electronics* **5**, 735 (2022).
- [88] A. Bose, N. J. Schreiber, R. Jain, D.-F. Shao, H. P. Nair, J. Sun, X. S. Zhang, D. A. Muller, E. Y. Tsymlal, D. G. Schlom, and D. C. Ralph, “Tilted spin current generated by the collinear antiferromagnet ruthenium dioxide,” *Nature Electronics* **5**, 267 (2022).
- [89] J. Liu, J. Zhan, T. Li, J. Liu, S. Cheng, Y. Shi, L. Deng, M. Zhang, C. Li, J. Ding, Q. Jiang, M. Ye, Z. Liu, Z. Jiang, S. Wang, Q. Li, Y. Xie, Y. Wang, S. Qiao, J. Wen, Y. Sun, and D. Shen, “Absence of altermagnetic spin splitting character in rutile oxide RuO_2 ,” arXiv e-

- prints (2024), [arXiv:2409.13504 \[cond-mat.mtrl-sci\]](https://arxiv.org/abs/2409.13504).
- [90] H.-Y. Ma, M. Hu, N. Li, J. Liu, W. Yao, J.-F. Jia, and J. Liu, “Multifunctional antiferromagnetic materials with giant piezomagnetism and noncollinear spin current,” *Nat. Commun.* **12**, 1 (2021).
- [91] F. Ferrari and R. Valenti, “Altermagnetism on the Shastry-Sutherland lattice,” arXiv e-prints (2024), [arXiv:2408.00841 \[cond-mat.str-el\]](https://arxiv.org/abs/2408.00841).
- [92] J. A. Sobral, S. Mandal, and M. S. Scheurer, “Fractionalized Altermagnets: from neighboring and altermagnetic spin-liquids to fractionalized spin-orbit coupling,” arXiv e-prints (2024), [arXiv:2410.10949 \[cond-mat.str-el\]](https://arxiv.org/abs/2410.10949).
- [93] E. Pavarini, I. Dasgupta, T. Saha-Dasgupta, O. Jepsen, and O. K. Andersen, “Band-structure trend in hole-doped cuprates and correlation with t_{cmax} ,” *Phys. Rev. Lett.* **87**, 047003 (2001).
- [94] C. C. Tsuei and J. R. Kirtley, “Pairing symmetry in cuprate superconductors,” *Rev. Mod. Phys.* **72**, 969 (2000).
- [95] M. E. Simon and C. M. Varma, “Detection and implications of a time-reversal breaking state in underdoped cuprates,” *Phys. Rev. Lett.* **89**, 247003 (2002).
- [96] C. M. Varma, “Non-fermi-liquid states and pairing instability of a general model of copper oxide metals,” *Phys. Rev. B* **55**, 14554 (1997).
- [97] M. S. Scheurer and S. Sachdev, “Orbital currents in insulating and doped antiferromagnets,” *Phys. Rev. B* **98**, 235126 (2018).
- [98] T. Fukui, Y. Hatsugai, and H. Suzuki, “Chern numbers in discretized brillouin zone: Efficient method of computing (spin) hall conductances,” *Journal of the Physical Society of Japan* **74**, 1674 (2005).
- [99] R. Zhao, G.-D. Xie, M. L. N. Chen, Z. Lan, Z. Huang, and W. E. I. Sha, “First-principle calculation of chern number in gyrotropic photonic crystals,” *Opt. Express* **28**, 4638 (2020).
- [100] S. Korrapati, S. Nandy, and S. Tewari, “Nonlinear thermoelectric response induced by berry curvature quadrupole in systems with broken time-reversal symmetry,” [arXiv preprint arXiv:2401.08155 \(2024\)](https://arxiv.org/abs/2401.08155).
- [101] S. Sankar, R. Liu, C.-P. Zhang, Q.-F. Li, C. Chen, X.-J. Gao, J. Zheng, Y.-H. Lin, K. Qian, R.-P. Yu, X. Zhang, Z. Y. Meng, K. T. Law, Q. Shao, and B. Jäck, “Experimental evidence for a berry curvature quadrupole in an antiferromagnet,” *Phys. Rev. X* **14**, 021046 (2024).
- [102] I. Sodemann and L. Fu, “Quantum nonlinear hall effect induced by berry curvature dipole in time-reversal invariant materials,” *Phys. Rev. Lett.* **115**, 216806 (2015).
- [103] M. Ezawa, “Intrinsic nonlinear conductivity induced by quantum geometry in altermagnets and measurement of the in-plane néel vector,” [arXiv preprint arXiv:2409.09241 \(2024\)](https://arxiv.org/abs/2409.09241).
- [104] Y. A. Bychkov and É. I. Rashba, “Properties of a 2d electron gas with lifted spectral degeneracy,” *JETP lett* **39**, 78 (1984).

Appendix A: Different adatom configurations

In this appendix, we demonstrate the robustness of our conclusions in the main text by varying the form of the superlattice modulation. The first configuration that we explore here can be thought of as placing the adatoms between two sites. In this situation, we assume that $W = 0$ but $\delta t_{ij} \neq 0$ for ij forming a square superlattice. We show in Fig. 4(a) a possible arrangement of adatoms (red links) to realize this superlattice. In Fig. 4(b) we can already see the resulting out-of-plane magnetic field component and that, again, the orbital altermagnet emerges but with a different periodicity (i.e., different unit cell size) compared to the examples in the main text. Here, however, there is a major difference from the case with adatoms on top of sites: the order parameter modulation is “indirect”, i.e., we are not directly tuning the chemical potential. The drawback of this is that we need to keep μ close to the region with $s + id$ phase.

As mentioned in the main text, we can also use a rectangular superlattice to modulate the superconductivity and still obtain an orbital altermagnet. Now, however, $C_{4z}\mathcal{T}$ and σ_v are no longer present. In Fig. 5(a) we illustrate the unit cell for this type of superlattice, while in (b) we show the respective out-of-plane component of the magnetic field.

Appendix B: Starting from homogeneous s -wave

Alternatively to what we show in the main text, one could start from a homogeneous system with extended s -wave superconductivity and use an adatom superlattice to modulate Δ to have a local preference for a d -wave symmetric order parameter. There are two ways to modify the system considered in the main text to achieve this modulation: one is to consider electron doped systems ($\mu > 0$) and the second way is to use $W < 0$ for hole doped systems. Here we use the first route to illustrate this alternative method.

Similarly to the main text Fig. 2, in Fig. 6(a) we show the phase diagram without any adatoms. In (b) we observe the resulting Δ_{ij} for $\mu = 3.5$ and notice that it has the “dual” behavior from Fig. 2(b), i.e., now Δ_{ij} is stronger in the links between sites with adatoms rather than the link between sites without adatoms. In (c), we show the respective current profile which is the same as the one in Fig. 2(c). For Fig. 6(d) we observe the biggest difference

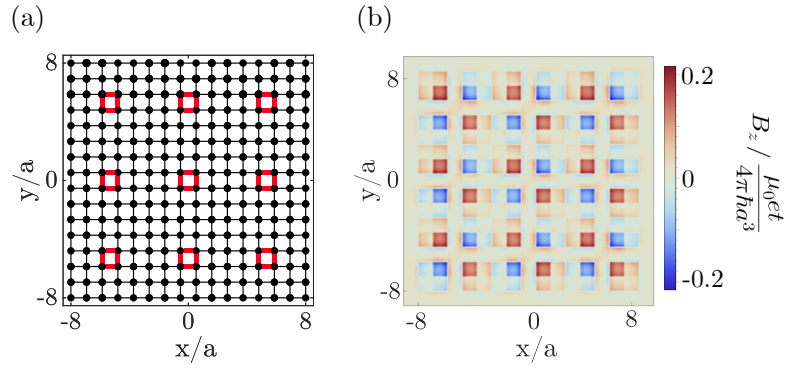


FIG. 4: (a) Adatom placement affecting the hopping t_{ij} on the red links. Here $\delta t_{ij} = -0.3$ instead of $t_{ij} = 1$, which is valid for the black links. (b) Out-of-plane magnetic field component at $z = 0.1a$. Here $\mu = 1.8$.

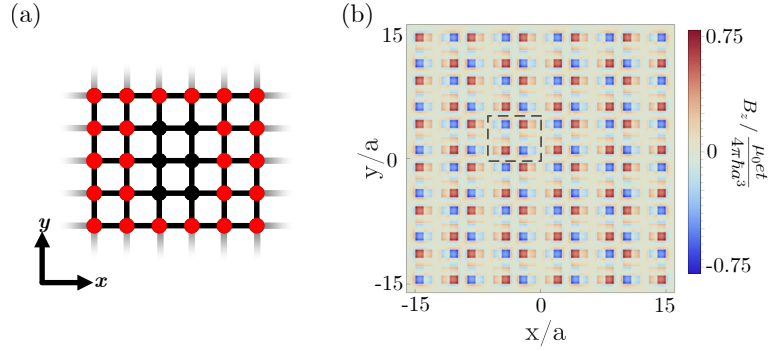


FIG. 5: (a) Unit cell for a rectangular adatom superlattice. The red points show where the adatoms are placed. (b) Out-of-plane magnetic field component at $z = 0.1a$. Here $\mu = -0.5$ and $W = 2$. The dashed line shows an unit cell.

when comparing to the corresponding plot in Fig. 2(d). Now the presence of loop currents is centered around the s -wave region as anticipated. We can also see that for the d -wave region there are also currents. This happens because in that region W now connects the d -wave for $\mu > 0$ with the s -wave region for $\mu < 0$. Whenever there are orbital currents, the superconductor and currents exhibit the same altermagnetic symmetries.

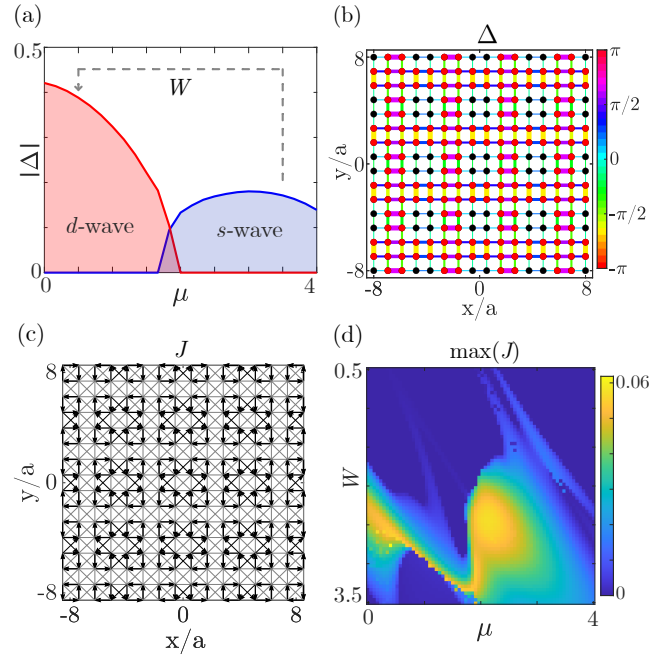


FIG. 6: (a) Phase diagram without adatoms for electron doping, featuring d -, extended s -wave, and $s \pm id$ superconductivity. The dashed line shows the two phases that are “connected” through a local adatom modulation W . (b) Adatom configuration (red dots) on top of our superconducting lattice (black dots). The colors and width of the bonds represent the complex phase and magnitude of the resulting Δ_{ij} . (c) Respective currents, with only those larger than 5% of the maximum current shown for clarity. (d) Maximal current for different μ and W showing the robustness of the altermagnet phase.